NUMERICAL MODELING OF THE MEDIUM-DENSITY FIBERBOARD HOT PRESSING PROCESS, PART 1: COUPLED HEAT AND MASS TRANSFER MODEL

Zanin Kavazović†

Postdoctoral Fellow
E-mail: zanin.kavazovic.1@ulaval.ca

Jean Deteix

Research Associate
Groupe Interdisciplinaire de Recherche en Éléments Finis
Département de Mathématiques et de Statistique
1045, Avenue de la Médecine, Université Laval
Québec, QC, Canada, G1V 0A6
E-mail: deteix@giref.ulaval.ca

Alain Cloutier*†

Professor
Centre de Recherche sur le Bois
Département des Sciences du Bois et de la Forêt
2425, Rue de la Terrasse, Université Laval
Québec, QC, Canada G1V 0A6
E-mail: alain.cloutier@sbf.ulaval.ca

André Fortin

Professor
Groupe Interdisciplinaire de Recherche en Éléments Finis
Département de Mathématiques et de Statistique
1045, avenue de la Médecine, Université Laval
Québec, QC, Canada G1V 0A6
E-mail: afortin@giref.ulaval.ca

Abstract.   A mathematical model describing heat and moisture transfer during hot pressing of medium-density fiberboard mats is presented. The model is based on conservation of energy, air mass, and water vapor mass, resulting in a three-dimensional unsteady-state problem in which mat properties and state variables vary in time and space. The conservation equations are expressed as functions of the three state variables: temperature, air pressure, and vapor pressure. The model includes conductive and convective heat transfer, phase change of water, and convective and diffusive mass transfer. Resin curing kinetics and latent heat associated with phase change of water are also taken into account. The closing of the batch press and development of the density profile are taken into account by imposing a predefined time- and space-dependent density profile. Calculations are carried out on reference geometry, and mathematical details relevant to the transfer from actual to reference geometry are presented. The system is discretized in space by the finite element method and in time by the Euler implicit scheme. The results exhibit good agreement with experimental measurements and provide information on variables of interest such as total gas pressure, temperature, moisture content, RH, and resin cure.

Keywords: Mathematical model, hot pressing, coupled heat and mass transfer, finite element method, resin cure kinetics, reference domain.

---

* Corresponding author
† SWST member

INTRODUCTION

Hot pressing of medium-density fiberboard (MDF) is a complex process involving several mechanical and heat and mass transfer phenomena in the fiber mat. Numerous efforts have been made by researchers to better understand heat and mass transfer phenomena occurring in wood-based panel mats during hot pressing. A comprehensive literature review can be found in Bolton and Humphrey (1988) and Humphrey (1982). Among the first researchers proposing an integrated approach were Kavvouras (1977), Humphrey (1982), and Humphrey and Bolton (1989). The first multidimensional heat and moisture transfer model was probably proposed by Humphrey (1982). A series of articles describing the physics involved in hot pressing particleboard and presenting typical predictive results followed (Bolton et al 1989a, 1989b, 1989c; Humphrey and Bolton 1989). Work by Bolton and Humphrey is the foundation on which the comprehensive model proposed by Thömen and Humphrey (2006) was developed.

Different heat and mass transfer models describing the hot pressing process of wood-based composite panels such as MDF, oriented strandboard, and particleboard have been proposed by Carvalho and Costa (1998), Thömen (2000), Nigro and Storti (2001), Zombori (2001), García (2002), Zombori et al (2003), Dai and Yu (2004), Pereira et al (2006), Thömen and Humphrey (2006), and Vidal Bastías (2006) just to mention a few. Ultimately, all heat and mass transfer models are based on conservation of energy and conservation of mass of air and water vapor (Zombori et al 2003; Dai and Yu 2004; Thömen and Humphrey 2006). To these conservation laws, one can add the cure kinetics equation of the adhesive system to predict the evolution of resin cure (Loxton et al 2003; Zombori et al 2003). Local thermodynamic equilibrium between mat moisture content and water vapor is assumed, and the relationship among equilibrium moisture content (EMC), RH, and temperature (EMC-RH-T) needs to be described. To predict hygrothermal conditions within the mat, several complex and nonlinear moisture sorption models are available in the literature (Malmquist 1958; Nelson 1983; Wu 1999; Dai and Yu 2004; Vidal Bastías and Cloutier 2005). The study by Vidal Bastías and Cloutier (2005) showed that the Malmquist (1958) sorption model gives the best overall fit to experimental EMC in the temperature range corresponding to MDF mat hot pressing.

The greatest amount of heat is supplied to the mat by heated press platens. Heat released by the exothermic reaction of resin polymerization is also taken into account as well as the energy associated with the phase change of water. Because moisture content of the mat is below the FSP, only bound water is considered in the model (Dai and Yu 2004). Hence, in the energy balance equation, the heat of phase change involves latent heat of desorption and evaporation (bound water to vapor) and latent heat of condensation and adsorption (water vapor to bound water) (Nigro and Storti 2001; Zombori et al 2003; Dai and Yu 2004; Thömen and Humphrey 2006). Heat in the fiber mat is transferred both by conductive heat flux (modeled by Fourier's law) and convective heat flux (heat transported by gas flow through the mat).

Gas in the mat is regarded as an ideal gas and assumed to be a mixture of air and water vapor (Thömen and Humphrey 2006). Gas flow is assumed to be laminar, and the total gas pressure gradient generates a convective gas flow, which is modeled by Darcy's law. Diffusive fluxes of air and water vapor are both driven by their partial pressure gradients and are described by Fick's law.

Furthermore, the complexity and strong coupled nature of the physical processes involved during heat and mass transfer are widely recognized in the literature (Bolton and Humphrey 1988; Humphrey and Bolton 1989; Carvalho and Costa 1998; Nigro and Storti 2001; Zombori et al 2003; Dai and Yu 2004; Thömen and Humphrey 2006). However, a clear description of how the coupling procedure is incorporated in the numerical resolution strategy is most often omitted.

Use of a finite element method and an implicit time scheme is not frequent in the literature. The only work using this approach that we found is Nigro and Storti (2001). Most authors use finite difference discretizations with explicit and thus conditionally stable time integration schemes. This approach involves the use of smaller time steps to satisfy stability conditions (eg time step of 0.005 s used by Yu et al [2007]).

Despite the literature already available, it is often difficult to reproduce the numerical results presented. From the finite element simulation point of view, it is important to be specific about the partial differential equations that constitute the model, the imposed boundary conditions, the material properties, and the numerical methods used to solve the problem. The aim of this work was to present and solve such a model based on a set of mathematical equations modeling the complex phenomena of heat and moisture transfer during batch hot pressing of MDF mats. At each time step, the system of coupled equations is solved on a reference domain. Mathematical details of the transformation from the actual to the reference geometry are explained. We also describe in detail how the full coupling of conservation equations is achieved from modeling and numerical simulation standpoints. We used a finite element code called MEF++ developed by the Groupe Interdisciplinaire de Recherche en Éléments Finis, Laval University, Quebec, Canada. This code is designed to facilitate changes of input data such as reference geometry, material properties, predefined density profiles, time schemes, linear or quadratic finite element approximation of the state variables, time step, and mesh adaptation. Development of such a model contributes to better understanding of the complex physical phenomena involved in the hot pressing process of MDF and other wood-based composite panels. It will also provide the industry with an analytical tool to optimize the hot pressing process and to develop innovative products.

MATERIALS AND METHODS

When developing a mathematical model to simulate physical phenomena, it is important to compare results produced by the model with experimental data. This was done to validate our numerical model.

Materials

Six MDF mats were produced in the laboratory for model validation purposes. Temperature and gas pressure were measured in the fiber mat during the pressing process at the center of the vertical panel plane. Temperature was measured at three points across mat thickness (at the core, at one-fourth thickness, and at the surface), whereas total gas pressure was measured at the core and the surface. Refined softwood MDF fibers were obtained from the Uniboard MDF La-Baie plant (Ville de La-Baie, Quebec, Canada).

Methods

Panel manufacturing. Fibers were a blend of about 90% black spruce (*Picea mariana*) and 10% balsam fir (*Abies balsamea*). Fibers at 6.5% initial MC were blended with 12% (fiber oven-dry weight basis) urea–formaldehyde (UF) resin and 1% wax in a laboratory rotary drum blender. Initial moisture content of the furnish was 12%. Six MDF panels with dimensions of $560 \times 460 \times 13$ mm and a target density of 750 kg/m^3 at 8% moisture content were produced in a Dieffenbacher (Eppingen, Germany) laboratory batch press equipped with a PressMAN measurement and control system. The press platens were at 203°C. The pressing schedule of 335 s was divided into five steps. The initial mat thickness of about 182 mm was decreased to 140% of final thickness in the first 35 s (Step 1). The press remained in this position for the next 15 s (Step 2) followed by the second compression lasting 110 s at the end of which the mat reached its final thickness of 13 mm (Step 3). The hot platens remained in this position for the next 110 s (Step 4). The final step (Step 5) was the venting period (65 s) during which the press was slowly opened and reached 107% of final panel thickness at 335 s. The curve presenting evolution of mat thickness with time is shown in Fig 1a.
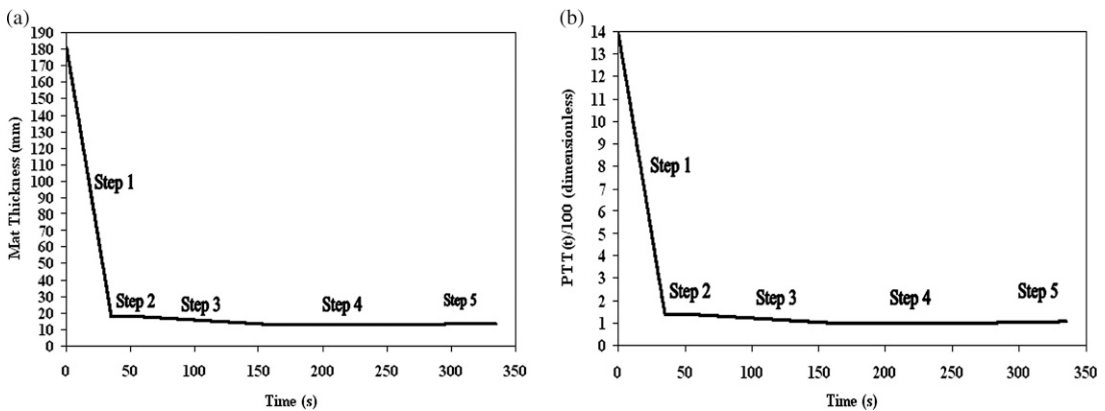
Figure 1.   Evolution of (a) mat thickness and (b) normalized percentage of mat target thickness (PTT[t]).

Model development. The proposed model is based on conservation principles leading to three governing conservation equations: conservation of energy, mass of air, and mass of water vapor (Zombori et al 2003; Dai and Yu 2004; Thömen and Humphrey 2006). This results in a three-dimensional unsteady-state mathematical–physical model in which the fiber mat properties and state variables vary in space and time. The three state variables of the model are temperature, air pressure, and vapor pressure. The conservation equations are expressed as functions of these three main variables. Furthermore, resin cure is predicted by considering the cure kinetics equation of the adhesive system as part of the energy balance equation (Loxton et al 2003; Zombori et al 2003; Dai and Yu 2004; Yu et al 2007). Malmquist's sorption isotherm model is used to describe dependence of the mat moisture content on temperature and RH.

Useful information on expressions and equations describing material properties, sorption model, and resin cure kinetics are taken from available literature (Appendix 1). Calculations were carried out on reference geometry, and effects of evolving domain geometry were accounted for by transferring equations and material properties from the evolving actual geometry to reference geometry.

Overall approach and assumptions. All mats were formed using the same raw materials and pressed using the same pressing schedule to pro-duce panels of the same dimensions. Bound water was assumed to be in equilibrium with water vapor in the lumens and in the mat voids. Local thermodynamic equilibrium was assumed at every point of the fiber mat, and the relationship among local moisture content, RH, and temperature was described by the sorption isotherm. Hence, the three state variables of the model were temperature, air pressure, and vapor pressure. All material properties of the fiber mat were taken from available literature (subsequently described and shown in Appendix 1), and none was obtained from panels produced in our laboratory.

Our model presents similarities with those published by Dai and Yu (2004) and Thömen and Humphrey (2006). However, in our approach, we also take into account the effect of compression on global mat geometry. Press closing (Fig 1) is considered, and the effect of changing mat thickness on the material properties (thermal conductivity, gas permeability, and porosity) is also accounted for.

The current study focuses on the heat and moisture transfer phenomena involved in hot pressing of MDF wood fiber mats. Rheology of mat consolidation was not explicitly considered. Consequently, the complex dynamical interactions between heat and moisture and rheological parameters involved during hot pressing were not taken into account. We are aware that this simplification may impact the results. A numerical coupling between the mechanical and the heat

and mass transfer models will be presented in Part 2 of this study. Nevertheless, in this work, a realistic mat vertical density profile was used during simulation runs (Appendices 2 and 3; Fig 2) (Kavazović et al 2010) to update the local heat and moisture transfer properties and porosity of the mat. Usually, instantaneous closing of the press is assumed. In our case, development of
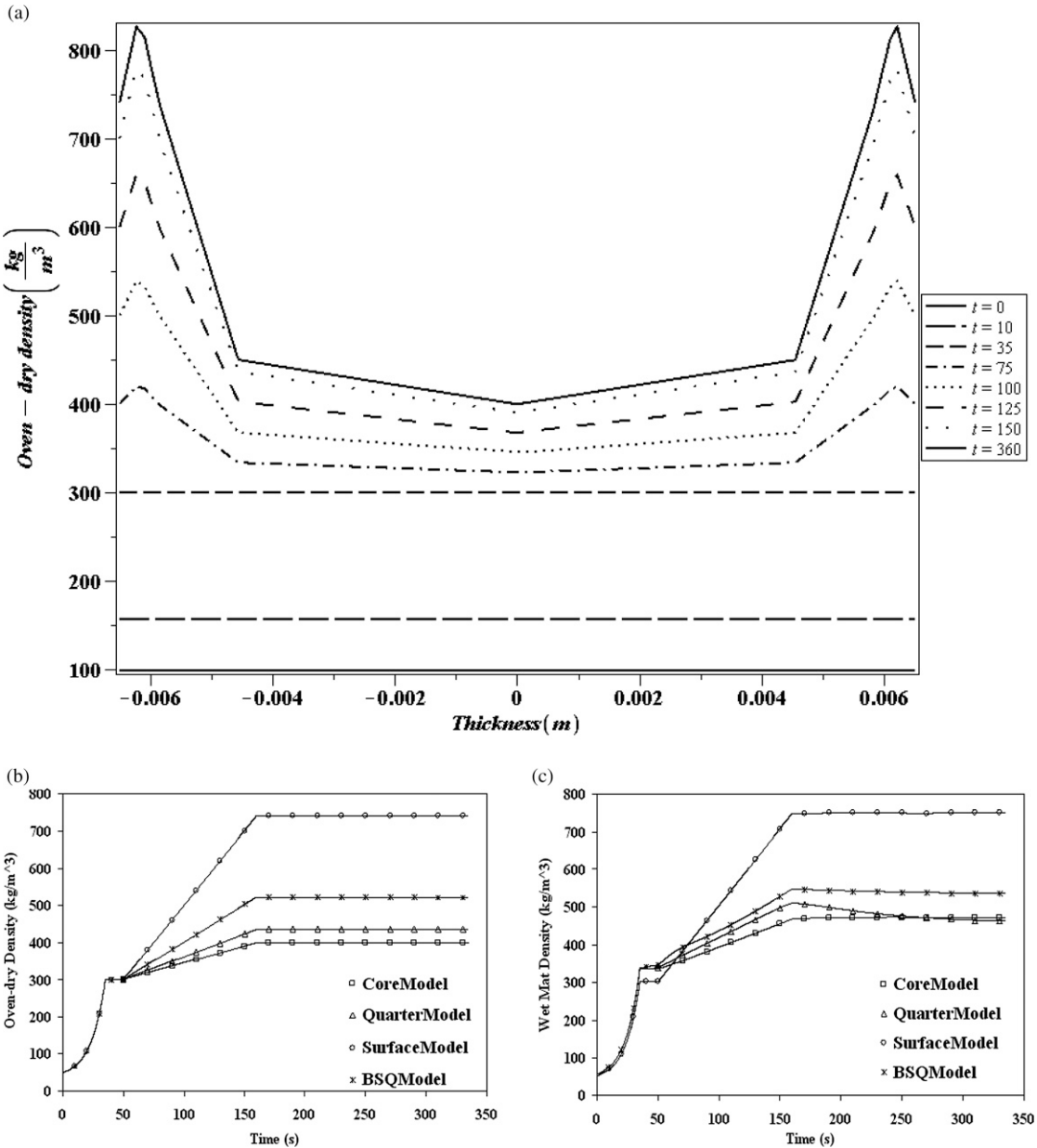

Figure 2.   (a) Evolution of a space- and time-dependent predefined oven-dry density profile used in calculations: vertical density profile in the centerline of the mat at different moments in time. Evolution of (b) predefined oven-dry density profile, values at four points in the vertical centerline (BSQ = middle point between surface and quarter); (c) wet density profile at four points in the vertical centerline calculated by $\rho_{Mat} = \rho_{OD}\,(1 + M)$.

the vertical density profile is taken into account by a time- and space-dependent expression (Appendix 2; Fig 2a) based on results presented by Wang and Winistorfer (2000), Winistorfer et al (2000), and Wang et al (2001, 2004). Generally, the vertical density profile of MDF panels exhibits a common M-shaped profile with higher density close to the surface and lower density in the core (Carvalho et al 2001, 2003; Wang et al 2001). It is frequently observed that the transition region from low to high density is rather thin (Carvalho et al 2001, 2003; Wang et al 2001). This characteristic M-shaped density profile (Fig 2a) is attributed to interactions between the heat and mass transfer phenomena and mechanical compression of the mat (Dai and Yu 2004). Furthermore, the evolution of oven-dry density at four representative points located in the vertical central plan of the mat (Fig 3c) is presented in Fig 2b.

The porosity of the mat was calculated by the formula presented by Siau (1984) as $\Phi = 1 - \frac{\rho_{OD}}{1530}$ and was thus time- and space-dependent.

It was assumed that initial mat moisture content was uniform throughout the thickness. The contribution of resin cure to heat and mass transfer was also taken into account. All results for the coupled three-dimensional mathematical model of heat and moisture transfer were obtained by finite element numerical simulations. The mass of oven-dry fiber material in each control region was assumed constant, and a control region of constant volume was considered (Thömen 2000; Thömen and Humphrey 2006).

Conservation Equations

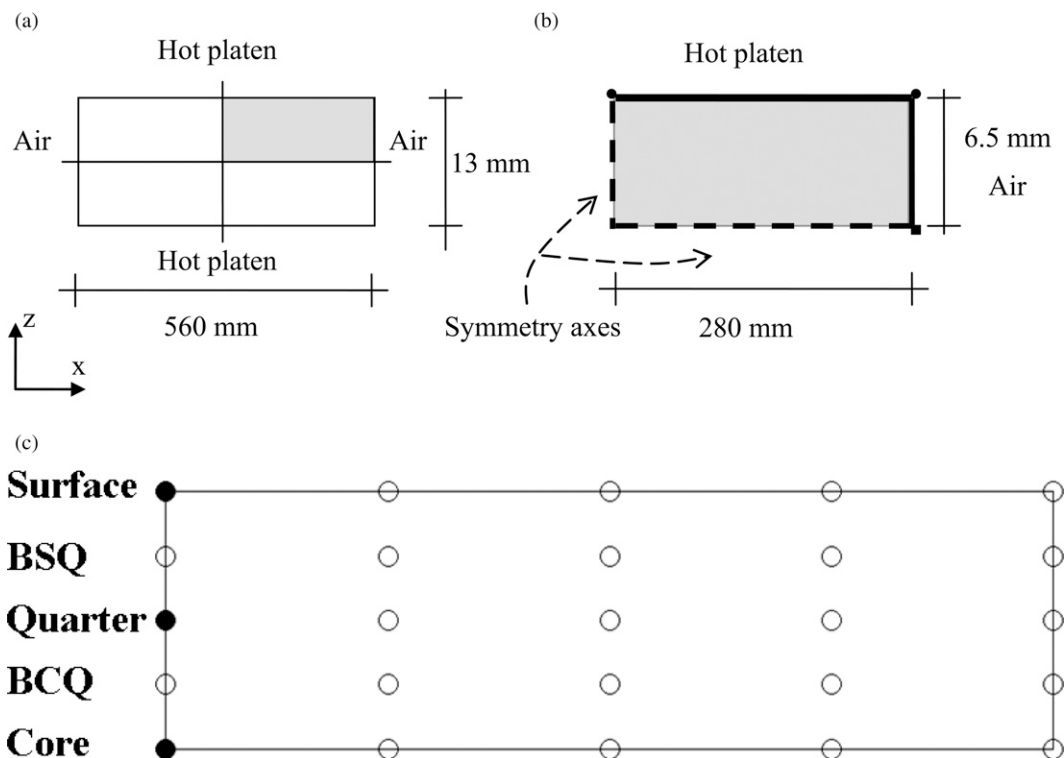When developing conservation equations, one should account for overall rate of change and

Figure 3.   (a) Full two-dimensional (2D) geometry of a fiber mat; (b) computational domain in 2D (one-fourth of the full geometry); (c) symmetry x-z (width-thickness) plane with equidistant tracing points (BSQ, between surface and quarter; BCQ, between center and quarter).

consider total derivative. Air, water vapor, and gas mixture are considered ideal gases and obey the ideal gas law. Movement of air and vapor mass is dependent on both bulk flow of the gas phase (convection generated by the gradient of total gas pressure and modeled by Darcy's law) and molecular diffusion of air and vapor within the gas phase (diffusion created by the gradient of partial air and vapor pressure modeled by Fick's law). Molecular diffusion translates the tendency to homogenize the gas phase. Given that the mat moisture content is significantly below the FSP, only bound water is present in the mat (Dai and Yu 2004).

Mass conservation of air. During hot pressing of MDF panels, no air is generated nor consumed. Hence, there is no source nor sink term in the conservation equation. Therefore, variations of air mass within a control volume of the mat are solely dependent on bulk flow of the gas phase and molecular diffusion of the air. Thus, the following equation expresses the conservation of air mass:

$$
\frac{d(\rho_a \Phi)}{dt} - \nabla \cdot \left(\left[\frac{\rho_a}{\mu} K_p \right] \cdot \nabla P \right)
$$
$$
- \nabla \cdot \left(\left[\frac{M_a}{RT} D_{eff} \right] \cdot \nabla P_a \right) = 0 \quad (1)
$$

Mass conservation of water vapor. Variations of water vapor mass within a control volume of the mat depended on bulk flow of the gas phase, molecular diffusion of the vapor within the gas phase, and evaporation (condensation) phenomena. Indeed, during hot pressing, bound water present in the MDF mat will partially evaporate in regions of high temperature and thus produce water vapor. Conversely, in cooler regions, condensation of water vapor may occur and increase bound water content. Evaporation of bound water can be seen as a source term for vapor, and condensation of water vapor is considered a sink. Bound water evaporation is equivalent to loss of bound water caused by moisture content decrease in time (García 2002), and condensation of vapor is equivalent to gain of bound water caused by

moisture content increase in time. Hence, the source and the sink terms of water vapor are both modeled by the following expression: $-\rho_{OD} \frac{dM}{dt}$ and the sign of $\frac{dM}{dt}$ determines if evaporation $\left(\frac{dM}{dt} < 0 \right)$ or condensation $\left(\frac{dM}{dt} > 0 \right)$ is taking place (García 2002; Thömen and Humphrey 2006). Therefore, the equation expressing conservation of water vapor mass is

$$
\frac{d(\rho_v \Phi)}{dt} - \nabla \cdot \left(\left[\frac{\rho_v}{\mu} K_p \right] \cdot \nabla P \right)
$$
$$
- \nabla \cdot \left(\left[\frac{M_v}{RT} D_{eff} \right] \cdot \nabla P_v \right) = -\rho_{OD} \frac{dM}{dt} \quad (2)
$$

Conservation of energy. Within the mat, heat is transferred by conduction (conductive heat flux) in the solid phase and convection in the gaseous phase (bulk flow and molecular diffusion). Energy associated with phase change (evaporation and condensation) is modeled by the expression $\left[H_{fg} + (C_{bw} - C_v)T \right] \rho_{OD} \frac{dM}{dt}$ (Thömen and Humphrey 2006; Humphrey and Bolton 1989; Thömen and Humphrey 2003; Dai and Yu 2004). Heat generated by the exothermic reaction of resin polymerization (Q_r) acts as an energy source. Hence, energy conservation of the system is expressed by

$$
\rho_{OD} \frac{d}{dt} [C_{Mat}T] + \frac{d}{dt} [C_a T \rho_a \Phi + C_v T \rho_v \Phi]
$$
$$
- \nabla \cdot (K_T \cdot \nabla T) - \nabla \cdot \left(\left[(\rho_a C_a + \rho_v C_v) \frac{T}{\mu} K_p \right] \cdot \nabla P \right)
$$
$$
- \nabla \cdot \left(\left[\frac{C_a M_a}{R} D_{eff} \right] \cdot \nabla P_a \right)
$$
$$
- \nabla \cdot \left(\left[\frac{C_v M_v}{R} D_{eff} \right] \cdot \nabla P_v \right)
$$
$$
= Q_r + \left[H_{fg} + (C_{bw} - C_v)T \right] \rho_{OD} \frac{dM}{dt} \quad (3)
$$

(see Nomenclature and Appendices 1 and 2 for definitions of variables and expressions). A model for cure kinetics of resin and energy (Q_r) related to resin polymerization is subsequently discussed.

Numerical Model of Heat and Mass Transfer in Fiber Mat

Our mathematical model can be seen as a generalization of the model proposed by Thömen and Humphrey (2006). Because the model is based on conservation of mass of air and water vapor and of energy, it is expressed in terms of the three state variables: partial air pressure (P_a), partial water vapor pressure (P_v), and temperature (T). Therefore, the model is formed by these three highly nonlinear conservation equations (Eqs 1, 2, and 3), which are strongly coupled. Also, time derivatives in each of the three conservation equations represent overall rate of change expressed by the total derivative.

Because the three state variables (P_a, P_v, T) depend on t, when the chain rule is for instance applied to $\frac{dM}{dt}$, one can replace it by the following expression:

$$\frac{dM}{dt} = \frac{\partial M}{\partial t} + \frac{\partial M}{\partial P_a} \frac{\partial P_a}{\partial t} + \frac{\partial M}{\partial P_v} \frac{\partial P_v}{\partial t} + \frac{\partial M}{\partial T} \frac{\partial T}{\partial t} \quad (4)$$

The same development was applied to other time derivatives included in the model.

Resin Cure Kinetics

We assumed a uniform distribution of resin throughout the fiber mat. In the laboratory experiments, UF thermosetting resin was used as the adhesive system. Several models of cure kinetics for different resin systems are available in the literature (Harper et al 2001; Xing et al 2004; Liang and Chandrashekhara 2006). The curing reaction of UF resin is assumed to have *n*th-order kinetics (Park et al 2008), and the extent of the resin cure α (ratio of cured resin mass to initial mass of uncured resin) is modeled by the following ordinary differential equation in which the temperature field T is in Kelvin:

$$\frac{d\alpha}{dt} = A \cdot \exp\left\{-\frac{E_a}{R \cdot T}\right\} \cdot (1 - \alpha)^n$$
$$\alpha(0) = 0 \quad (5)$$

The variable α takes values between 0 (no resin has yet been polymerized) and 1 (all available resin has been polymerized) (Liang and Chandrashekhara 2006). Reaction rate $\left(\frac{d\alpha}{dt}\right)$ is higher at higher temperatures, whereas the function $(1 - \alpha)^n$ describes the decrease of reaction rate as α increases and reactants are consumed. Values of the coefficients come from Xing (2003) and Xing et al (2004). Hence, the Arrhenius collision frequency factor $A = \exp(17)$ [1/s] (number of collisions that need to occur in a unit time to carry out the reaction), the Arrhenius activation energy $E_a = 7 \times 10^4$ J/mole (energy needed to carry the reaction), and the order of the reaction $n = 1.2$.

When solving Eq 5 for α, the temperature field T is assumed to be known. Given the initial condition $\alpha(0) = 0$, the analytical solution of Eq 5 with $n \neq 1$ is

$$\alpha(t) = 1 - \left[1 + \exp\left\{-\frac{E_a}{R \cdot T}\right\} \cdot A \cdot (n-1) \cdot t\right]^{\frac{1}{1-n}} \quad (6)$$

The reaction rate Q_r is used in the source term of the energy conservation equation (Eq 3). Indeed, Q_r represents heat generated by the exothermic reaction of resin polymerization. It is given by the following relation:

$$Q_r = \rho_r \cdot H_r \cdot \frac{d\alpha}{dt} \quad (7)$$

Hence,

$$Q_r = \rho_r \cdot H_r \cdot A \cdot \exp\left\{-\frac{E_a}{R \cdot T}\right\} \cdot (1 - \alpha)^n \quad (8)$$

where H_r is total heat released during the entire course of the polymerization reaction (latent heat of polymerization estimated at 10^5 J/kg by Xing [2003]) and ρ_r is the resin density expressed as the ratio of solid resin mass to total volume. Because the UF resin content of the fiber mat is 12% in this study, the corresponding mass of solid resin is given by 0.12 times the mass of oven-dry fibers, ie $\rho_r = 0.12 \, \rho_{OD}$.

Sorption Model

Following Dai and Yu (2004), we assume that local isothermal sorptive equilibrium exists among mat moisture content, RH, and temperature. The initial mat moisture content is assumed to be uniform throughout thickness and is set to 0.12. Experimental measurements of moisture content and RH during hot pressing are still not possible. However, the evolution of these variables can be predicted and monitored using an appropriate sorption model. Vidal Bastías and Cloutier (2005) compared several of the most frequently used sorption models. Their study showed that Malmquist's sorption model gives the best overall fit to EMC data. This model was therefore used in our numerical simulations. It expresses dimensionless moisture content M as a function of absolute temperature T and dimensionless relative humidity h:

$$M_{Malmquist} = \frac{MS}{1 + N\left(\frac{1}{h} - 1\right)^{\frac{I}{3}}} \qquad (9)$$

where MS, N, and I are second-order polynomials of the absolute temperature T defined as follows (Vidal Bastías and Cloutier 2005):

$$MS = 0.40221 - 9.736 \cdot 10^{-5} \cdot T - 5.8964 \cdot 10^{-7} \cdot T^2 \qquad (10)$$

$$N = -2.6939 + 0.018552 \cdot T - 2.1825 \cdot 10^{-6} \cdot T^2 \qquad (11)$$

$$I = 2.2885 - 0.0016742 \cdot T + 2.0637 \cdot 10^{-6} \cdot T^2 \qquad (12)$$

Finite Element Solution Strategy

An integrated approach considering simultaneously all important variables during hot pressing was proposed by Kavvouras (1977), Humphrey (1982), and Bolton and Humphrey (1988). Our solution strategy is quite different from what has traditionally been done. Indeed, for each of the three conservation equations, a finite element method discretization was performed in space, whereas the time derivatives were calculated using the stable Euler implicit scheme. This combination allowed for larger time steps (a time step of 0.1 s was used in this study) and decreased the calculation burden. Each state variable was discretized by Q1 (bilinear quadrangles) finite element (Bathe 1982; Reddy 2006). To address the nonlinearity of the system of coupled equations, at each time step, Newton's method was used (Nigro and Storti 2001), predicting the evolution of the state variables in space. Derivatives for the Jacobian matrix were explicitly computed, whereas Nigro and Storti (2001) used a finite difference approximation. However, at each time step and for each nonlinear iteration, the three nonlinear equations forming our coupled heat and mass transfer system were solved simultaneously, preserving the full coupling between them.

It has been common practice to keep local conditions and properties constant during a given time step (Thömen 2000; Thömen and Humphrey 2003). We, however, adopted a different approach. Within each time step, all local conditions and mat material properties were updated at each nonlinear iteration. We believe that this is a better numerical approach, and our code is able to deal easily with this level of complexity. At each time step, an average of four iterations of Newton's method were performed to reach convergence to 10^{-5} in the residual norm.

Computational Domain

Our mathematical model is three-dimensional (3D). However, at this stage, it will be applied on a two-dimensional (2D) geometry to decrease calculation time. Nevertheless, in Part 2 of this study, numerical results obtained with a global model on 3D geometry will be presented.

A daylight delay (the time necessary for the top platen to touch the mat) creating asymmetric distribution of internal mat conditions in the thickness direction was ignored. We followed a common path proposed in the literature and took advantage of the symmetry (Carvalho and Costa 1998; Carvalho et al 2001, 2003; Nigro

and Storti 2001; Thömen and Humphrey 2003; Dai and Yu 2004; Pereira et al 2006; Thömen and Humphrey 2006; Yu et al 2007). Hence, our computational domain represents a quarter of the full 2D geometry with the symmetry plans presented in Fig 3a and b. It was meshed with a 16×16 grid with 256 homogeneous rectangular elements. A discussion on grid size and its influence on numerical results will be presented in Part 2 of this study.

At different stages of the pressing process, the mat has different thickness values and its material properties change during compression. In this study, we worked on a reference domain: 280 mm (mat's half length in the x direction) × 6.5 mm (mat's half final thickness in the z direction). Thus, the transfer of material properties and the equations from a real-world evolving domain to the reference domain must be done. Subsequently, we explain the procedure to properly achieve this task.

Figure 3c shows a reference domain (width–thickness plane). Black dots represent locations where thermocouples (surface, quarter, and core) and pressure probes (surface and core) were installed to monitor the temperature and gas pressure. Also, points in the vertical centerline between

surface and quarter (BSQ) and between core and quarter (BCQ) as well as locations identified by empty circles were used as additional numerical tracing points for all variables.

Boundary Conditions

Appropriate boundary conditions are needed to properly solve the system constituted by Eqs 1, 2, and 3. The temperature evolution of the surface in contact with the hot platen (Fig 4a) was imposed by a Dirichlet boundary condition based on data obtained during in situ laboratory experiments. The surface in contact with the hot platen includes the two end vertices illustrated by black dots in Fig 3b. Also, the following fluxes were considered at the boundaries:

$$\text{Air flux: } q_{Pa} = -\left(\frac{\rho_a}{\mu} K_p \cdot \nabla P\right) - \left(\frac{M_a}{RT} D_{eff} \cdot \nabla P_a\right) \tag{13}$$

$$\text{Vapor flux: } q_{Pv} = -\left(\frac{\rho_v}{\mu} K_p \cdot \nabla P\right)$$
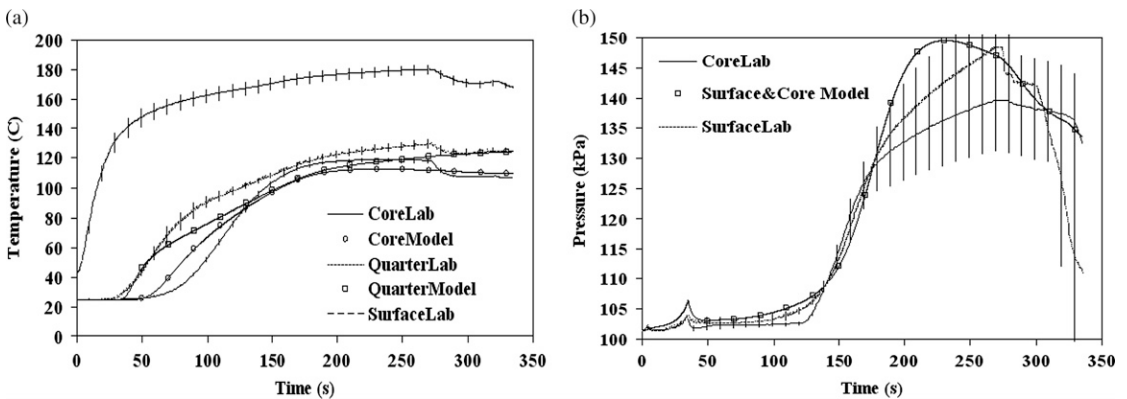$$- \left(\frac{M_v}{RT} D_{eff} \cdot \nabla P_v\right) \tag{14}$$

Figure 4.   (a) Temperature evolution in time (measurements at the surface, core, and one-fourth of the thickness and numerically predicted results at the core and one-fourth of the thickness). (b) Total gas pressure evolution in time (measurements and numerical results at the surface and core). The curve labeled surface and core model was obtained by numerical simulation, and the two others were measured in the laboratory. In all figures, special symbols such as □, o, *, ◇, □ are used to identify the different curves and do not represent experimental data unless the contrary is explicitly indicated. Vertical bars represent standard deviation from the mean value.

Heat flux: $q_T = -(K_T \cdot \nabla T)$

$$-\left(\frac{T(\rho_a C_a + \rho_v C_v)}{\mu} K_p \cdot \nabla P\right)$$

$$-\left(\frac{C_a M_a}{R} D_{eff} \cdot \nabla P_a\right)$$

$$-\left(\frac{C_v M_v}{R} D_{eff} \cdot \nabla P_v\right) \qquad (15)$$

The hot platen is assumed impervious to gas, and therefore $q_{Pa} = 0$ and $q_{Pv} = 0$. Symmetry conditions are imposed ($q_T = 0$, $q_{Pa} = 0$, $q_{Pv} = 0$) on the two symmetry axes illustrated by dashed lines in Fig 3b. On the external edge in contact with ambient air, the following convection boundary conditions are imposed for the three state variables, air pressure, vapor pressure, and temperature, respectively:

$$q_{Pa} \cdot \vec{n} = -h_p \frac{\rho_a}{\mu}(P - P_{amb}) - h_{pa} \frac{\rho_a}{P_a}(P_a - P_{a\,amb})$$
$$(16)$$

$$q_{Pv} \cdot \vec{n} = -h_p \frac{\rho_v}{\mu}(P - P_{amb}) - h_{pv} \frac{\rho_v}{P_v}(P_v - P_{v\,amb})$$
$$(17)$$

$$q_T \cdot \vec{n} = -h_T(T - T_{amb})$$
$$- h_p \frac{T(\rho_a C_a + \rho_v C_v)}{\mu}(P - P_{amb})$$
$$- h_{pa} \frac{C_a M_a}{R}(P_a - P_{a\,amb})$$
$$- h_{pv} \frac{C_v M_v}{R}(P_v - P_{v\,amb}) \qquad (18)$$

where $\vec{n}$ is the outward unit normal vector and h_T and h_p are the convective heat and mass transfer coefficients, respectively, associated with the external boundary (Zombori 2001; Vidal Bastías 2006). In Fig 3, the external edge is the right side edge of the rectangular domain and is represented by a continuous black line including the black square (Fig 3b). The main mode of mass transfer between the mat and the environment is the gas bulk flow (Zombori et al 2004) generated by the difference in total gas pressure within and outside the mat. Diffusion generated by the difference in

partial vapor pressure within and outside the mat plays a secondary role (Zombori et al 2004).

Thermal Conductivity of Mat

Thermal conductivity increases with increase of density, temperature, and moisture content of the fiber mat. We used the expression proposed by Thömen and Humphrey (2006) for thermal conductivity of the fiber mat ($K_{Tx} = K_{Ty} = 1.5 \cdot K_{Tz}$) where

$$K_{Tz} = K_{T030} + \Delta K_T \qquad (19)$$

$$K_{T030} = 4.38 \times 10^{-2} + 4.63 \times 10^{-5} \cdot \rho_{OD} + 4.86 \times 10^{-8} \cdot \rho^2_{OD} \qquad (20)$$

and

$$\Delta K_T = 0.49M + \left(1.1 \times 10^{-4} + 4.3 \times 10^{-3} \cdot M\right) \cdot (T - 303.15) \qquad (21)$$

The variables K_{Tx}, K_{Ty}, and K_{Tz} are diagonal components of thermal conductivity tensor K_T and represent, respectively, thermal conductivity in the two horizontal directions and in the thickness. K_{T030} is thermal conductivity measured at 0% M and 30°C, and ΔK_T is the correction term accounting for moisture content and temperature effects on thermal conductivity.

Specific Gas Permeability of Mat

Samples prepared from consolidated panels with an adhesive content of 11% were used by von Haas et al (1998) to determine the permeability of fiber, particle, and strand mats with densities varying from 200-1200 kg/m³. In our study, analytical expression for the specific gas permeability tensor K_p for the MDF mats is based on curve fitting of experimental data proposed by von Haas et al (1998). The in-plane permeability (K_{px} and K_{py}) and the cross-sectional permeability (K_{pz}) of MDF fiber mats are both described by the following expression:

$$\exp\left(\frac{1}{A}\right) \quad \text{where} \quad A = a + b \cdot \rho_{Mat} + \frac{c}{\ln(\rho_{Mat})}$$
$$(22)$$

and the coefficients to determine K_{px} and K_{py} are $a = -0.041$, $b = 9.51 \cdot 10^{-6}$, $c = -0.015$ and those for K_{pz} are $a = -0.037$, $b = 1.1 \cdot 10^{-5}$, $c = -0.037$.

Transfer to Reference Domain

Generic approach. Let Ω be a real-world domain where the coordinates of a given point are (x,y,z), and let $\widehat{\Omega}$ be a reference domain (where the calculations are carried out) where the coordinates of a given point are $(\hat{x},\hat{y},\hat{z})$. The invertible function $\overrightarrow{G} : \widehat{\Omega} \to \Omega$, $\overrightarrow{G}(\hat{x},\hat{y},\hat{z}) = (x,y,z)$ transfers a point from the reference domain to a real-world domain. Its inverse function, $\overrightarrow{H} = \overrightarrow{G^{-1}}$: $\Omega \to \widehat{\Omega}$, $\overrightarrow{H}(x,y,z) = (\hat{x},\hat{y},\hat{z})$, transfers a point from the real-world domain to the reference domain. If we express the real-world coordinates as a function of the reference domain coordinates, one can write $x = g_1(\hat{x},\hat{y},\hat{z})$; $y = g_2(\hat{x},\hat{y},\hat{z})$; $z = g_3(\hat{x},\hat{y},\hat{z})$ and we have

$$\overrightarrow{G}(\hat{x},\hat{y},\hat{z}) = [g_1(\hat{x},\hat{y},\hat{z}), g_2(\hat{x},\hat{y},\hat{z}), g_3(\hat{x},\hat{y},\hat{z})]$$
$$= (x,y,z) \qquad (23)$$

Similarly, one can express the reference domain coordinates as a function of the real-world coordinates: $\hat{x} = h_1(x,y,z)$; $\hat{y} = h_2(x,y,z)$; $\hat{z} = h_3(x,y,z)$ and get

$$\overrightarrow{H}(x,y,z) = [h_1(x,y,z), h_2(x,y,z), h_3(x,y,z)]$$
$$= (\hat{x},\hat{y},\hat{z}) \qquad (24)$$

Let $F = F(x,y,z)$ be any scalar function expressed on the real-world domain Ω and $\widehat{F} = \widehat{F}(\hat{x},\hat{y},\hat{z})$ the same scalar function expressed on the reference domain $\widehat{\Omega}$. Then, the following derivatives can be calculated and written in matrix notation:

$$
\begin{bmatrix} \frac{\partial \widehat{F}}{\partial \hat{x}} \\ \frac{\partial \widehat{F}}{\partial \hat{y}} \\ \frac{\partial \widehat{F}}{\partial \hat{z}} \end{bmatrix} = \begin{bmatrix} \frac{\partial g_1}{\partial \hat{x}} & \frac{\partial g_2}{\partial \hat{x}} & \frac{\partial g_3}{\partial \hat{x}} \\ \frac{\partial g_1}{\partial \hat{y}} & \frac{\partial g_2}{\partial \hat{y}} & \frac{\partial g_3}{\partial \hat{y}} \\ \frac{\partial g_1}{\partial \hat{z}} & \frac{\partial g_2}{\partial \hat{z}} & \frac{\partial g_3}{\partial \hat{z}} \end{bmatrix} \begin{bmatrix} \frac{\partial F}{\partial x} \\ \frac{\partial F}{\partial y} \\ \frac{\partial F}{\partial z} \end{bmatrix} \text{ and}
$$

$$
\begin{bmatrix} \frac{\partial F}{\partial x} \\ \frac{\partial F}{\partial y} \\ \frac{\partial F}{\partial z} \end{bmatrix} = \begin{bmatrix} \frac{\partial h_1}{\partial x} & \frac{\partial h_2}{\partial x} & \frac{\partial h_3}{\partial x} \\ \frac{\partial h_1}{\partial y} & \frac{\partial h_2}{\partial y} & \frac{\partial h_3}{\partial y} \\ \frac{\partial h_1}{\partial z} & \frac{\partial h_2}{\partial z} & \frac{\partial h_3}{\partial z} \end{bmatrix} \begin{bmatrix} \frac{\partial \widehat{F}}{\partial \hat{x}} \\ \frac{\partial \widehat{F}}{\partial \hat{y}} \\ \frac{\partial \widehat{F}}{\partial \hat{z}} \end{bmatrix} \quad (25)
$$

or written in a more compact way:

$$\widehat{\nabla}\widehat{F} = \left[\widehat{\nabla}\overrightarrow{G}\right]^T \nabla F \text{ and } \nabla F = \left[\nabla \overrightarrow{H}\right]^T \widehat{\nabla}\widehat{F} \quad (26)$$

and one easily comes to the conclusion $\left[\nabla \overrightarrow{H}\right]^{-1} = \left[\widehat{\nabla}\overrightarrow{G}\right]$. From the finite element point of view, the transfer of equations is not code-invasive. Indeed, in each integral of the weak formulation, the coefficients are multiplied by an appropriate Jacobian and the material properties represented by a tensor K on the real-world domain are represented by the tensor $\left[\nabla \overrightarrow{H}\right]\widehat{K}\left[\nabla \overrightarrow{H}\right]^T$ on the reference domain. That methodology is applied to each of the three conservation equations of our model (Eqs 1, 2, 3). See Kavazović (2011) for an illustration of the transfer of calculations from the real-world domain to the reference domain applied to a generic conservation equation.

Mat compression. During the pressing process, thickness of the mat decreases as a function of the press closing schedule. Mat target thickness (*MTT*) is known in advance (*MTT* = 13 mm in our case). When symmetry is assumed, half of the *MTT* is used in the calculations (6.5 mm). The press closing schedule is only time-dependent and can be expressed in terms of percentage of *MTT* and named *PTT*(*t*). In our simulation runs, *PTT*(*t*) is known (Appendix 3; Fig 1b). Therefore, one can express the evolution of the real mat thickness (*RMT*) in terms of *MTT* and *PTT*(*t*) as follows:

$$RMT(t) = \frac{PTT(t)}{100} MTT \qquad (27)$$

Because the calculations are performed on an arbitrary but fixed reference domain $\widehat{\Omega}$, its thickness (*RDT*: reference domain thickness) is also known. Thus, the following useful expression can be defined:

$$\lambda(t) = \frac{RMT(t)}{RDT} \qquad (28)$$

During pressing, the greatest variations in mat dimensions occur in the thickness direction, whereas variations in the *x* and *y* directions can

be considered negligible. Thus, the transformation function $\overrightarrow{G}$ and the associated Jacobian J have the following expressions:

$$\overrightarrow{G}(\hat{x},\hat{y},\hat{z}) = (\hat{x},\hat{y},\lambda(t)\hat{z}) = (x,y,z) \text{ and}$$

$$J = \det\left(\left[\nabla\overrightarrow{H}\right]^{-1}\right) = \det\left(\left[\hat{\nabla}\overrightarrow{G}\right]\right) = \lambda(t) \quad (29)$$

Hence, for any tensor $\widehat{K}$ defined by $\widehat{K} = \begin{bmatrix} \hat{k}_{11} & \hat{k}_{12} & \hat{k}_{13} \\ \hat{k}_{21} & \hat{k}_{22} & \hat{k}_{23} \\ \hat{k}_{31} & \hat{k}_{32} & \hat{k}_{33} \end{bmatrix}$, we have

$$\left[\nabla\overrightarrow{H}\right]\widehat{K}\left[\nabla\overrightarrow{H}\right]^{T} = \begin{bmatrix} \hat{k}_{11} & \hat{k}_{12} & \frac{\hat{k}_{13}}{\lambda(t)} \\ \hat{k}_{21} & \hat{k}_{22} & \frac{\hat{k}_{23}}{\lambda(t)} \\ \frac{\hat{k}_{31}}{\lambda(t)} & \frac{\hat{k}_{32}}{\lambda(t)} & \frac{\hat{k}_{33}}{\lambda^{2}(t)} \end{bmatrix} \quad (30)$$

More details can be found in Kavazović (2011). This transfer strategy was applied to several different reference domains to test the independency of the results on the reference geometry. All numerical tests were successful and gave the same results.

RESULTS AND DISCUSSION

The numerical model used here is based solely on heat and mass transfer mechanisms, and the influence of changing moisture content and temperature on rheological mechanisms was not considered. The numerically predicted solutions depended on several heat and mass transfer properties of the fiber mat, and most of these properties are only known to a limited degree of precision, especially under the conditions prevailing during hot pressing. Also, the fiber mat material properties including thermal conductivity, gas permeability, and porosity were taken from the literature and were not determined from the specific material used to make our panels. This can explain some of the discrepancies between the model and the experimental results.

The temperature measurements are presented together with numerically predicted results in Fig 4a. The curve labeled *SurfaceLab* is temperature measured in the laboratory at the surface in contact with the hot platen and was imposed as a Dirichlet boundary condition for T at the surface. However, curves labeled *CoreModel* and *QuarterModel* were obtained by numerical simulation and represent the temperature at the center and at one-fourth of the thickness, respectively (Fig 3c). Numerically predicted temperature at the core and at one-fourth of thickness (Fig 4a) closely followed the evolution of in situ measurements. In particular, the plateau temperatures and the time when they are reached appeared to be quite similar. The total gas pressure curves are shown in Fig 4b with standard deviation bars. In the second half of the pressing period, experimental measurements of total gas pressure exhibited more scattering with coefficients of variation of approximately 6% (Fig 4b). Numerically predicted total gas pressure appeared to be constant through mat thickness. Hence, predicted values of gas pressure at the core and surface of the mat (Fig 3c) were equal and both curves were superimposed (curve labeled *Surface&CoreModel*) and are thus identified by the same symbol in Fig 4b. The model captured major trends and gave good quality results that were somewhat closer to experimental results than those presented by Zombori et al (2004) and Thömen and Humphrey (2006). Compared with experimental measurements, numerically predicted results for temperature and gas pressure exhibited satisfactory behavior. However, the absence of the total gas pressure gradient in the vertical center plane is interesting. The same phenomenon is observed by most of the investigators presenting numerically predicted total gas pressure during hot pressing of wood-based panels (Carvalho and Costa 1998; Thömen 2000; Carvalho et al 2003; Zombori et al 2003; Pereira et al 2006; Thömen and Humphrey 2006; Yu et al 2007). Nevertheless, we and these authors observed the development of a significant horizontal total gas pressure gradient, especially in the core, driving the gas out of the mat.

Figure 5 presents numerical predictions of the evolution of moisture content (M) (Fig 5a) and RH (*RH*) (Fig 5b) in the mat during hot pressing.
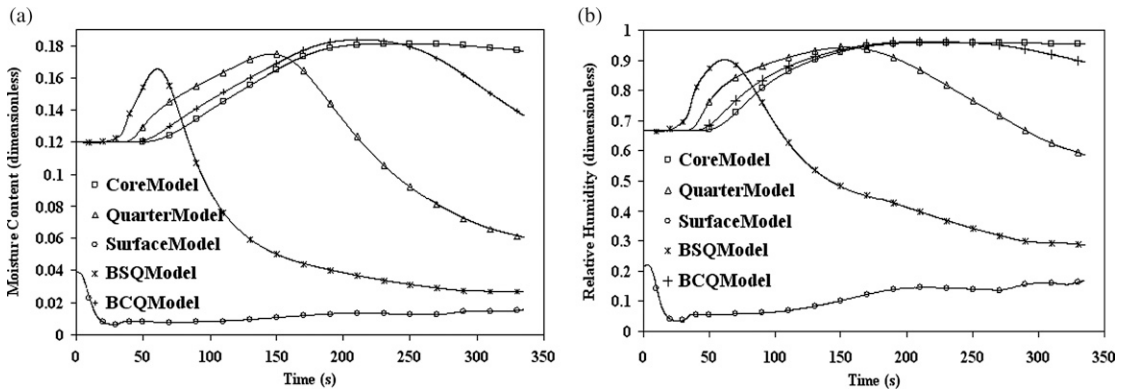
Figure 5.   Numerical predictions of moisture content (MC) and RH at five equidistant points in the vertical centerline of the mat (BSQ, between surface and quarter; BCQ, between center and quarter). Evolution of (a) MC and (b) RH.

Results are presented for five equidistant points laying in the vertical centerline of the mat (Fig 3c): at the core, at one-fourth of the thickness, at the surface, and at the midpoints between the core and one-fourth of the thickness (BCQ) and between the surface and one-fourth of the thickness (BSQ). The sorption isotherm model relates moisture content to RH and temperature. Therefore, it is not surprising that very similar behavior occurred in curves representing the *M* evolution and the *RH* evolution in the mat. Comparable observations were also made by Yu et al (2007). Furthermore, from the early stages of the hot pressing process, surface temperature increased rapidly, causing evaporation of bound water and thus decreasing *M* and increasing gas pressure at the surface. This induced vapor flow toward the inner layers. Given that inner layers had lower temperature, water vapor condensed, and thus increased the local moisture content (Yu et al 2007). A sequence of peaks of local moisture content presented in Fig 5a clearly shows movement of *M* from the surface region toward the core layer. As a consequence, the amount of bound water in the core region of the mat increased with time. It took a large amount of energy and time to evaporate the accumulated bound water. That explains the long-lasting temperature plateau in the core (Fig 4a).

Wet mat density is a function of oven-dry density and mat moisture content. As can be seen in Fig 2, time and space evolution of wet mat density was mostly influenced by the predefined oven-dry density profile (Fig 2b and 2c).

Figure 6 summarizes results obtained for partial air (P_a) and vapor (P_v) pressure at five representative locations (Fig 3c) in the vertical center plane. Figure 6a shows that, for the first 30 s of pressing, air pressure quickly dropped at the surface, whereas it remained almost stable in the inside layers. At the same time, because of the evaporation process taking place close to the hot surface, vapor pressure exhibited the opposite behavior; it increased at the surface and remained unchanged elsewhere (Fig 6b). This created vertical partial air and vapor pressure gradients. However, as the hot pressing process continued, air pressure rapidly decreased, which indicates that air was leaving the mat by the edges. As heat penetrated deeper into the mat, the amount of bound water evaporated gradually increased, causing a noticeable increase of vapor pressure. Hence, water vapor replaced air and occupied a large proportion of the gaseous phase. Higher temperature (more evaporation) and density (lower permeability) contributed to gas pressure build-up, especially in the core. Difference in gas pressure between the core and the edges resulted in gas flow in the panel plane. This agrees with observations made by Yu et al (2007).

Finally, Fig 7 summarizes numerical predictions at four representative locations (Fig 3c) of the
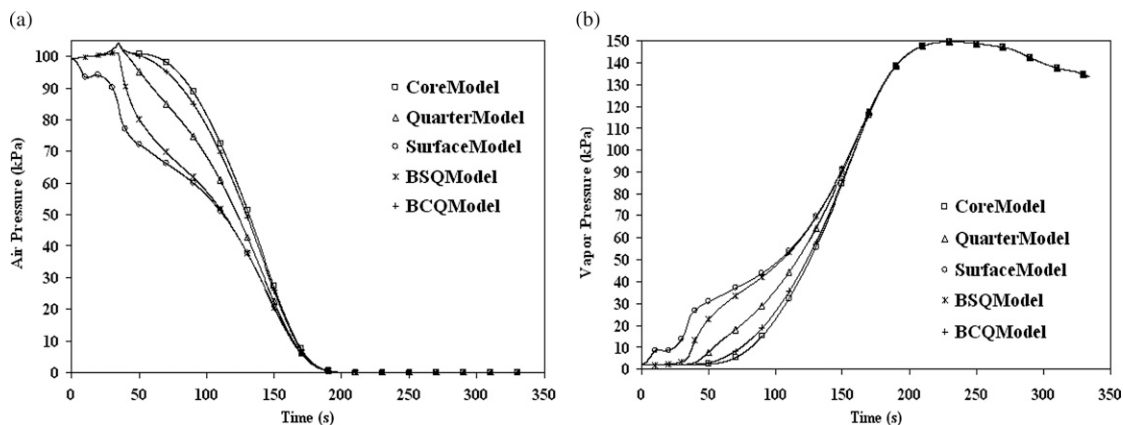
(a)

(b)

Figure 6.   Numerical predictions of partial air and vapor pressure at five equidistant points in the vertical centerline of the mat (BSQ, between surface and quarter; BCQ, between center and quarter). Evolution of (a) partial air pressure and (b) partial vapor pressure.
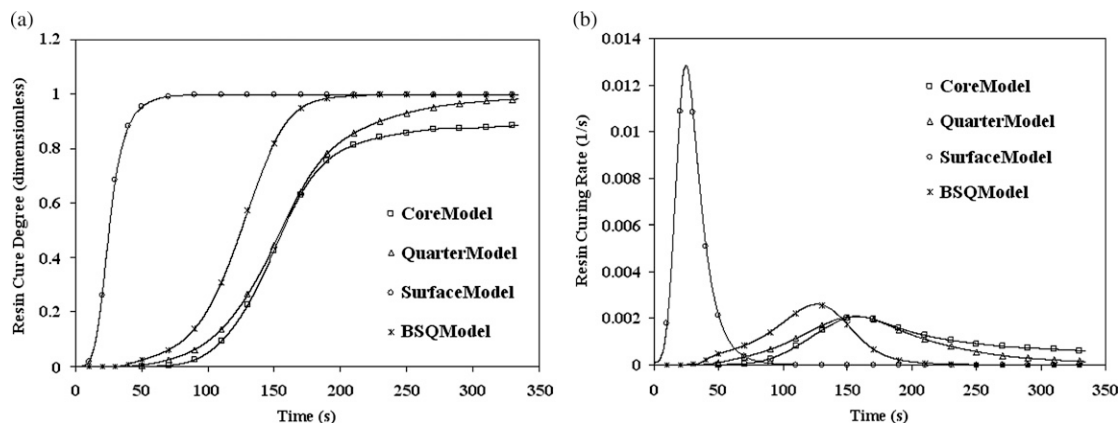
(a)

(b)

Figure 7.   Numerical predictions of degree of resin cure and resin curing rate at four points in the vertical centerline of the mat (BSQ, middle point between surface and quarter). Evolution of (a) resin cure degree and (b) resin curing rate.

degree of resin cure and the resin curing rate. As expected, at the beginning of the hot pressing process, the resin curing rate was highest at the surface (Fig 7b) resulting in the fastest increase in the resin cure degree, which rapidly reached its highest value (Fig 7a). Because of the high temperature, all available resin at the surface quickly polymerized. Then, the curing rate in that region quickly vanished. As the temperature of the layers closer to the core increased, the amount of cured resin also increased. That increased the degree of resin cure toward its

maximum value (Fig 7a). Of course, as the reactants were used up, the rate of resin cure consequently diminished and tended to zero (Fig 7b). These results agree with those presented by Yu et al (2007).

CONCLUSIONS

This study presents a detailed 3D mathematical approach to developing a physical–mathematical model for heat and mass transfer that occurs in MDF mats during hot pressing. The complex

nature and interactions of different physical phenomena are described by means of three strongly coupled and nonlinear conservation equations. These equations form a coherent system and are expressed as functions of the three state variables of the model, namely temperature, air pressure, and vapor pressure. Those equations also take into account the curing kinetics of UF resin, and Malmquist's model describes the sorption isotherm. Physical and heat and mass transfer properties of the fiber mat are also considered to be time- and position-dependent. The fully coupled system of governing nonlinear equations, discretized by the finite element method, is solved by Newton's method on a reference domain, and mathematical details of the transfer of those equations from a real-world domain to a reference domain are presented. Numerically predicted results for temperature and gas pressure exhibited good correspondence with experimental data. Also, the model provided good predictions of the evolution of moisture content, RH, partial air and vapor pressure, and extent of resin cure. Thus, the model provides a good and reasonably reliable insight into the complex dynamics of heat and mass transfer phenomena.

Nomenclature

t = time [s]

x = length [m]

y = width [m]

z = thickness [m]

T = temperature field [K], a state variable calculated by the model

P_a = partial air pressure [Pa], a state variable calculated by the model

P_v = partial vapor pressure [Pa], a state variable calculated by the model

P = total gas pressure [Pa]

M = moisture content [dimensionless]

h = relative humidity [dimensionless]

P_{vSAT} = saturated vapor pressure [Pa]

M_a = molar mass of air [kg/mol]

M_v = molar mass of water vapor [kg/mol]

R = universal gas constant [J/(mol·K)]

ρ_a = density of the air [kg/m^3]

ρ_v = density of the water vapor [kg/m^3]

ρ_{OD} = oven-dry density of the mat [kg/m^3] (see Appendix 2)

Φ = porosity of the mat [dimensionless]

ρ_{Mat} = wet density of the mat [kg/m^3]

K_T = thermal conductivity tensor [J/(m·s·K)]

K_p = tensor of specific (effective) gas permeability of the mat [m^3/m]

D_{eff} = tensor of effective diffusion coefficient [m^2/s]

D_{va} = binary molecular diffusion coefficient of the air–vapor gas mixture [m^2/s]

k_d = obstruction factor [dimensionless]

H_{fg} = latent heat of vaporization (desorption + evaporation of bound water; condensation + adsorption of water vapor) [J/kg]

C_{Mat} = mass specific heat capacity of the mat at current moisture content [J/(kg·K)]

C_a = mass specific heat capacity of air [J/(kg·K)]

C_v = mass specific heat capacity of water vapor [J/(kg·K)]

C_{bw} = mass specific heat capacity of the bound water [J/(kg·K)]

μ = dynamic viscosity of the air–vapor mixture [Pa·s]

μ_a = dynamic viscosity of the air [Pa·s]

μ_v = dynamic viscosity of the water vapor [Pa·s]

h_T = convective heat transfer coefficient associated with the external boundary [J/(m^2·s·K)]

h_p = convective mass transfer coefficient associated with the external boundary [m]

h_{pa} = diffusive air mass transfer coefficient associated with the external boundary [m/s]

h_{pv} = diffusive vapor mass transfer coefficient associated with the external boundary [m/s]

q_T = heat flux [J/(m^2·s)]

q_{Pa} = air flux [kg/(m^2·s)]

q_{Pv} = water vapor flux [kg/(m^2·s)]

EMC = equilibrium moisture content [dimensionless]

RH = relative humidity [dimensionless]

MTT = mat target thickness [m]

M_{init} = initial moisture content of the mat [dimensionless]

T_{init} = initial temperature of the mat [K]

h_{init} = initial value of relative humidity [dimensionless]

$P_{vSAT\ init}$ = initial value of saturated vapor pressure [Pa]

$P_{v\ init}$ = initial value of partial vapor pressure [Pa]

$P_{a\ init}$ = initial value of partial air pressure [Pa]

$T_{surface}$ = temperature at the surface in contact with the hot platen [K]

h_{amb} = relative humidity of ambient gas [dimensionless]

T_{amb} = temperature of the ambient gas [K]

$P_{vSAT\ amb}$ = saturated vapor pressure in ambient gas [Pa]

P_{amb} = ambient gas pressure [Pa]

$P_{v\ amb}$ = ambient vapor pressure [Pa]

$P_{a\ amb}$ = ambient air pressure [Pa]

REFERENCES

Bathe KJ (1982) Finite element procedures in engineering analysis. Prentice-Hall, Upper Saddle River, NJ. 735 pp.

Bolton AJ, Humphrey PE (1988) The hot pressing of dry-formed wood-based composites. Part I. A review of the literature identifying the primary physical process and the nature of their interaction. Holzforschung 42(6):403-406.

Bolton AJ, Humphrey PE, Kavvouras PK (1989a) The hot pressing of dry-formed wood-based composites. Part III. Predicted pressure and temperature variation with time and compared with experimental data for laboratory board. Holzforschung 43(4):265-274.

Bolton AJ, Humphrey PE, Kavvouras PK (1989b) The hot pressing of dry-formed wood-based composites. Part IV. Predicted variation of mattress moisture content with time. Holzforschung 43(5):345-349.

Bolton AJ, Humphrey PE, Kavvouras PK (1989c) The hot pressing of dry-formed wood-based composites. Part VI. The importance of stresses in the pressed mattress and their relevance to the minimisation of pressing time and the variability of board properties. Holzforschung 43(6):406-410.

Carvalho LM, Costa CAV (1998) Modeling and simulation of the hot-pressing process in the production of medium density fiberboard (MDF). Chem Eng Commun 170:1-21.

Carvalho LMH, Costa MRN, Costa CAV (2001) Modeling rheology in the hot-pressing of MDF: Comparison of mechanical models. Wood Fiber Sci 33(3):395-411.

Carvalho LMH, Costa MRN, Costa CAV (2003) A global model for the hot-pressing of MDF. Wood Sci Technol 37:241-258.

Dai C, Yu C (2004) Heat and mass transfer in wood composite panels during hot-pressing. Part 1. A physical–mathematical model. Wood Fiber Sci 36(4):585-597.

García P (2002) Three-dimensional heat and mass transfer during oriented strandboard hot-pressing. PhD thesis, University of British Columbia, Vancouver, BC, Canada. 254 pp.

Harper DP, Wolcott MP, Rials TG (2001) Evaluation of the cure kinetics of the wood/pMDI bondline. Int J Adhes Adhes 21:137-144.

Humphrey PE (1982) Physical aspects of wood particleboard manufacture. PhD thesis, University of Wales, Bangor, Wales, UK.

Humphrey PE, Bolton AJ (1989) The hot pressing of dry-formed wood-based composites. Part II. A simulation model for heat and moisture transfer and typical results. Holzforschung 43(3):199-206.

Kavazović Z (2011) Modélisation mathématique du pressage à chaud des panneaux MDF: Couplage du modèle mécanique avec le modèle couplé de transfert de chaleur et de masse. PhD thesis, Université Laval, Québec, Canada. 145 pp. http://www.giref.ulaval.ca/publications/memoires-et-theses.html (16 February 2012).

Kavazović Z, Deteix J, Cloutier A, Fortin A (2010) Sensitivity study of a numerical model of heat and mass transfer involved during the MDF hot pressing process. Wood Fiber Sci 42(2):1-20.

Kavvouras PK (1977) Fundamental process variables in particleboard manufacture. PhD thesis, University of Wales, UK. 156 pp.

Liang G, Chandrashekhara K (2006) Cure kinetics and rheology characterization of soy-based epoxy resin system. J Appl Polym Sci 102:3168-3180.

Loxton C, Thumm A, Grigsby WJ, Adams TA, Ede RM (2003) Resin distribution in medium density fiberboard. Quantification of UF resin distribution on blow line and

dry-blended MDF fiber and panels. Wood Fiber Sci 35(3):370-380.

Malmquist L (1958) Sorption a deformation of space. Svenska Traforskningsinstitutet Trateknik Meddelande 983, Stockholm, Sweden.

Nelson RM Jr. (1983) A model for sorption of water by cellulosic materials. Wood Fiber Sci 15(1):8-22.

Nigro N, Storti M (2001) Hot-pressing process modeling for medium density fiberboard (MDF). Int J Math Sci 26(12):713-729.

Park BD, Kang EC, Park JY (2008) Thermal curing behavior of modified urea-formaldehyde resin adhesives with two formaldehyde scavengers and their influence on adhesion performance. J Appl Polym Sci 110:1573-1580.

Pereira C, Carvalho LMH, Costa CAV (2006) Modeling the continuous hot-pressing of MDF. Wood Sci Technol 40:308-326.

Reddy JN (2006) An introduction to the finite element method. 3rd ed. McGraw Hill Higher Education. New York. 766 pp.

Siau J (1984) Transport processes in wood. Springer-Verlag. New York. 245 pp.

Thömen H (2000) Modeling the physical process in natural fiber composites during batch and continuous pressing. PhD thesis, Oregon State University, Corvallis, OR. 187 pp.

Thömen H, Humphrey PE (2003) Modeling the continuous pressing process for wood-based composites. Wood Fiber Sci 35(3):456-468.

Thömen H, Humphrey PE (2006) Modeling the physical process relevant during hot pressing of wood-based composites. Part 1. Heat and mass transfer. Holz Roh Werkst 64:1-10.

Vidal Bastías M (2006) Modélisation du pressage à chaud des panneaux de fibres de bois (MDF) par la méthode des éléments finis. PhD thesis, Univeristé Laval, Québec, Canada. 158 pp.

Vidal Bastías M, Cloutier A (2005) Evolution of wood sorption models for high temperatures. Maderas-Cienc Tecnol 7(2):145-158.

von Haas G, Steffen A, Fruhwald A (1998) Untersuchungen zur permeabilitat von faser- span- und OSB-Matten fur gase. Holz Roh Werkst 56:386-392.

Wang S, Winistorfer PM (2000) Fundamentals of vertical density profile formation in wood composites. Part 2. Methodology of vertical density formation under dynamic conditions. Wood Fiber Sci 32(2):220-238.

Wang S, Winistorfer PM, Young TM (2004) Fundamentals of vertical density profile formation in wood composites. Part 3. MDF density formation during hot-pressing. Wood Fiber Sci 36(1):17-25.

Wang S, Winistorfer PM, Young TM, Helton C (2001) Step-closing pressing on medium density fiberboard. Part 1. Influences on the vertical density profile. Holz Roh Werkst 59:19-26.

Winistorfer PM, Moschler WW Jr., Wang S, DePaula E, Bledsoe BL (2000) Fundamentals of vertical density profile formation in wood composites. Part 1. In-situ density measurement of the consolidation process. Wood Fiber Sci 32(2):209-219.

Wu Q (1999) Application of Nelson's sorption isotherm to wood composites and overlays. Wood Fiber Sci 31(2): 187-191.

Xing C (2003) Characterization of urea–formaldehyde resin efficiency affected by four factors in the manufacture of medium density fiberboard. PhD thesis, Université Laval, Québec, Canada. 198 pp.

Xing C, Riedl B, Cloutier A, He G (2004) The effect of urea–formaldehyde resin pre-cure on the internal bond of medium density fiberboard. Holz Roh Werkst 62:439-444.

Yu C, Dai C, Wang BJ (2007) Heat and mass transfer in wood composite panels during hot pressing. Part 3. Predicted variations and interactions of the pressing variables. Holzforschung 61:74-82.

Zombori BG (2001) Modeling the transient effects during the hot-pressing of wood-based composites. PhD thesis, Virginia Tech, Blacksburg, VA. 212 pp.

Zombori BG, Kamke FA, Watson LT (2003) Simulation of the internal conditions during the hot-pressing process. Wood Fiber Sci 35(1):2-23.

Zombori BG, Kamke FA, Watson LT (2004) Sensitivity analysis of internal mat environment during hot pressing. Wood Fiber Sci 36(2):195-209.

APPENDIX 1

Expressions of some parameters used in the calculations.

$$P = P_a + P_v : \text{Dalton's law}$$

M: defined at every point in the mat by a sorption model, we use Malmquist's sorption model as a reference

$$M_{Malmquist} = \frac{MS}{1 + N\left(\frac{1}{h} - 1\right)^{\frac{I}{3}}}$$

where MS, N, and I are second-order polynomials of absolute temperature T [K] given by

$$MS = 0.40221 - 9.736 \cdot 10^{-5} \cdot T - 5.8964 \cdot 10^{-7} \cdot T^2$$

$$N = -2.6939 + 0.018552 \cdot T - 2.1825 \cdot 10^{-6} \cdot T^2$$

$$I = 2.2885 - 0.0016742 \cdot T + 2.0637 \cdot 10^{-6} \cdot T^2$$

$$h = \frac{P_v}{P_{vSAT}};$$

$$P_{vSAT} = \exp\left\{53.421 - \frac{6516.3}{T} - 4.125 \cdot \ln(T)\right\}$$

(Kirchoff's formula)

$$M_a = 28.951 \cdot 10^{-3}; \; M_v = 18.015 \cdot 10^{-3};$$
$$R = 8.314472$$

$$\rho_a = \frac{M_a P_a}{RT} \text{ (ideal gas law)};$$
$$\rho_v = \frac{M_v P_v}{RT} \text{ (ideal gas law)}$$

$$\rho_{Mat} = \rho_{OD}(1 + M); \; \Phi = 1 - \frac{\rho_{OD}}{1530} \text{ (Siau 1984)}$$

$$D_{eff} = \frac{D_{va}}{k_d} I, \text{ where } I \text{ is identity tensor};$$

$$D_{va} = 2.6 \cdot 10^{-5} \cdot \left(\frac{101325}{P}\right) \cdot \left(\frac{T}{298.2}\right)^{1.75}$$

$$k_d = 0.334 \cdot e^A, \; A = 5.08 \cdot 10^{-3} \cdot \rho_{Mat}$$

$$H_{fg} = 2.511 \cdot 10^6 - 2.48 \cdot 10^3 \cdot (T - 273.15)$$
$$+ 1.172 \cdot 10^6 \cdot e^{-0.15 \cdot M \cdot 100}$$

$$C_{Mat} = \frac{1131 + 4.19 \cdot (T - 273.15) + 4190 \cdot M}{1 + M}$$

$$C_a = 1003.5; \; C_v = 1950; \; C_{bw} = C_{water} = 4190:$$
because of lack of data

$$\mu = \frac{P_a}{P}\mu_a + \frac{P_v}{P}\mu_v; \; \mu_a = \frac{1.37 \cdot 10^{-6} \cdot T^{1.5}}{T + 85.75};$$
$$\mu_v = \frac{1.12 \cdot 10^{-5} \cdot T^{1.5}}{T + 2937.85}$$

$$h_T = 0.35; \; h_p = 2 \cdot 10^{-11}; \; h_{pa} = 10^{-5}; \; h_{pv} = 10^{-5}$$

$$MTT = 0.013 \text{ m}; \; M_{init} = 0.12; \; T_{init} = 298.15$$

h_{init} calculated by Malmquist's formula

$$\frac{1}{h_{init}} = 1 + \left[\frac{1}{N_{init}}\left(\frac{MS_{init}}{M_{init}} - 1\right)\right]^{\frac{3}{I_{init}}}$$

where

$$MS_{init} = 0.40221 - 9.736 \cdot 10^{-5} \cdot T_{init}$$
$$- 5.8964 \cdot 10^{-7} \cdot T_{init}{}^2$$

$$N_{init} = -2.6939 + 0.018552 \cdot T_{init}$$
$$- 2.1825 \cdot 10^{-6} \cdot T_{init}{}^2$$

$$I_{init} = 2.2885 - 0.0016742 \cdot T_{init}$$
$$+ 2.0637 \cdot 10^{-6} \cdot T_{init}{}^2$$

$$P_{vSAT\,init} = \exp\left\{53.421 - \frac{6516.3}{T_{init}} - 4.125 \cdot \ln(T_{init})\right\};$$

$$P_{v\,init} = h_{init} \cdot P_{vSAT\,init}; \; P_{a\,init} = 101325 - P_{v\,init}$$

$T_{surface}$: temperature at the surface in contact with the hot platen; its evolution in time is imposed by the Dirichlet boundary condition, and the values are prescribed by measured experimental data (Figs 3 and 4a).

$$h_{amb} = 0.3$$

$T_{amb} = T_{surface}$: because the size of the mat is much smaller than the platens of the press, the temperature of the air surrounding the mat under compression is much higher than 298.15 K and is supposed to be equal to the temperature at the surface of the mat.

$$P_{vSATamb} = \exp\left\{53.421 - \frac{6516.3}{T_{amb}}\right.$$
$$\left. - 4.125 \cdot \ln(T_{amb})\right\}$$

$$P_{amb} = 101325; \; P_{v\,amb} = h_{amb} \cdot P_{vSAT\,amb};$$
$$P_{a\,amb} = P_{amb} - P_{v\,amb}$$

<div style="text-align:center">

APPENDIX 2

</div>

A predefined mat oven-dry vertical density profile (ρ_{OD} [kg/m^3]) was used for calculations. This profile is space- (z) and time- (t) dependent and is based on results presented by Wang and Winistorfer (2000). A similar approach was adopted by Kavazović et al (2010). The profile as a function of time and space (position in the thickness direction) is presented in Fig 2.

Because the symmetry of the vertical density profile is assumed in the thickness (z) direction, its mathematical expression represents half of the mat thickness. However, the density profile is divided into four sections in the z direction, and in each section, it is represented by a different function: LD = low-density section, MD = medium-density section, $HD1$ = first part of the high-density section, $HD2$ = second part of the high-density section.

$$\rho_{OD} = \left\{ \begin{array}{ll} LD & 0 \leq |z| \leq 0.00455 \\ MD & 0.00455 < |z| < 0.00585 \\ HD1 & 0.00585 \leq |z| \leq 0.006175 \\ HD2 & 0.006175 < |z| \leq 0.0065 \end{array} \right\}$$

where

$$LD = \left\{ \begin{array}{ll} 36.6 + 13 \cdot \exp(0.086 \cdot t) & 0 \leq t \leq 35 \\ 300 & 35 < t \leq 50 \\ 300 + (t - 50) \cdot (0.909091 + 99.9 \cdot |z|) & 50 < t \leq 160 \\ 400 + 10989.011 \cdot |z| & 160 < t \end{array} \right\}$$

$$MD = \left\{ TPLD + (|z| - 0.00455) \cdot \frac{(BPHD - TPLD)}{(0.00585 - 0.00455)} \quad 0 \leq t \right\}$$

$$TPLD = \left\{ \begin{array}{ll} 36.6 + 13 \cdot \exp(0.086 \cdot t) & 0 \leq t \leq 35 \\ 300 & 35 < t \leq 50 \\ 231.8182 + 1.3636 \cdot t & 50 < t \leq 160 \\ 450 & 160 < t \end{array} \right\}$$

$$BPHD = \left\{ \begin{array}{ll} 36.6 + 13 \cdot \exp(0.086 \cdot t) & 0 \leq t \leq 35 \\ 300 & 35 < t \leq 50 \\ 100 + 4 \cdot t & 50 < t \leq 160 \\ 740 & 160 < t \end{array} \right\}$$

$$HD1 = \left\{ \begin{array}{ll} 36.6 + 13 \cdot \exp(0.086 \cdot t) & 0 \leq t \leq 35 \\ 300 & 35 < t \leq 50 \\ 300 + (t - 50) \cdot (-12.3636 + 2797.2028 \cdot |z|) & 50 < t \leq 160 \\ -1060 + 3.077 \cdot 10^5 \cdot |z| & 160 < t \end{array} \right\}$$

$$HD2 = \left\{ \begin{array}{ll} 36.6 + 13 \cdot \exp(0.086 \cdot t) & 0 \leq t \leq 35 \\ 300 & 35 < t \leq 50 \\ 300 + (t - 50) \cdot (22.18182 \cdot |z|) & 50 < t \leq 160 \\ 2740 - 3.077 \cdot 10^5 \cdot |z| & 160 < t \end{array} \right\}$$

APPENDIX 3

The press closing schedule is a time-dependent function. It can be expressed in terms of the mat target thickness (*MTT*) as a percentage of *MTT* and named *PTT*(*t*). Figure 1 illustrates its evolution in time. For example, when the press is in the position corresponding to 140% of *MTT*, *PTT* = 140%. Then, actual thickness of the mat equals 140% · *MTT*/100% = 1.4 · *MTT*. The time evolution of *PTT*(*t*)/100% used for our simulations is given by the following expression:

$$\frac{PTT(t)}{100\%} = \begin{cases} 14 - 0.36 \cdot t & 0 \leq t \leq 35 \\ 1.4 & 35 < t \leq 50 \\ \dfrac{87}{55} - \dfrac{1}{275} \cdot t & 50 < t \leq 160 \\ 1 & 160 < t \leq 270 \\ \dfrac{461}{650} + \dfrac{7}{6500} \cdot t & 270 < t \leq 335 \end{cases}$$